Technical Article

Time-domain homogenisation of laminated ferromagnetic cores in finite-element models

Abstract — **The laminated ferromagnetic cores of electromagnetic devices are subjected to time-varying alternating fields that generate eddy currents and considerable losses with possible significant impact on their performance. These losses must therefore be correctly accounted for in early design stages or even in the control system, particularly with the actual trend towards increasing switching frequency of the driving power electronics. Versatile field models, such as finite elements, provide the desired degree of accuracy but quickly become prohibitive in terms of computational resources, notably in three-dimensional real-life converters. Numerous homogenisation techniques have been developed to achieve the best compromise between computational cost and accuracy.**

This technical article begins with an overview of the most commonly used homogenisation approaches for lamination stacks. We further provide the specific technical details of our time-domain homogenisation approach, based on a one-dimensional model of a single lamination, and its integration within a finite element formulation. As validation test cases, we consider: 1) a stacked ring core with in-plane currents and hysteretic behaviour; and 2) a two-dimensional finite-element model of a switched reluctance motor considering the eddy-current effects.

I. Introduction

Ferromagnetic cores of electrotechnical devices (inductors, transformers, rotating electrical machines, etc.) are typically laminated to limit the eddy-current losses due to time-varying alternating fields. Nonetheless, these losses, and the iron losses as a whole, may still jeopardise the device behaviour, besides the obvious effect on heating, efficiency and performance [1]. Moreover, the trend towards higher and higher frequencies in the power electronics that feed the devices makes the accurate consideration of dynamic effects in the steel sheets an absolute prerequisite in early design stages. The highly versatile standard finite elements (FE) guarantee, in theory, the desired accuracy. However, for real-life applications with complicated fully three-dimensional (3D) geometries, the brute-force approach implies invariably the fine discretisation of each separate lamination with mesh elements that must resolve the skin depth. This strict requirement gives rise to a huge system of equations that goes still to date far beyond practical computational capabilities.

The pragmatic and widespread *a posteriori* eddy-current (and iron) loss estimation, i.e. applying phenomenological material models [2, 3] to post-process 2D/3D FE static solutions with stacked iron cores assumed non-conducting and homogeneous blocks, may not be sufficient in the ever-increasing frequency context. Dedicated homogenisation techniques become thus an indispensable and viable alternative.

Many homogenisation-based approaches have been proposed for efficiently dealing with lamination stacks in FE models in the frequency and/or time domain, considering saturation (possibly hysteresis) or not, including perpendicularly incident flux or not. Without being exhaustive, we may refer to: anisotropic surrogate material laws [4, 5, 6, 7], embedded lower dimensional models [8, 9] which can be localised and generated on the fly [10], semi-analytical models or single-step algorithms [11, 12, 13], computational multiscale methods or two-step algorithms [14, 15, 16], and very recently, non-asymptotic homogenisation [17]. Multi-harmonic variants can be found as well [18, 19]. Some research groups have also experimented with reduced order model techniques, either circuit-based [20, 21, 22] or using snapshots [23].

Perfect insulation between the laminations is mostly assumed, i.e. the induced current density cancels in any lamination cross-section, the net current is zero. In practice net circulating currents may appear due to inter-lamination coating damage (edge burrs, welding process, conducting joints, etc.) [24, 25]. In the literature, we find different attempts to incorporate these short circuits in the homogenisation approaches. Obviously, these mostly local defects do not comply with the underlying spatial periodicity hypothesis. The short-circuited laminations are handled by means of hybrid models [26, 27, 28], a combination of subproblems [29], or with *ad hoc* single sheet models with net currents [30, 31]. The latter models work very well with localised short circuits [32].

Homogenisation methods accounting for hysteresis are mainly limited to time-harmonic analysis either a complex reluctivity [33], or a iterative scheme between the solutions of a 1D lamination problem and a 2D/3D problem [8]. In [34], a pragmatic two-step homogenisation approach is proposed. Inspired from the computational multiscale methods [15, 35], that are more accurate but also very computationally demanding, it generates an averaged constitutive relationship by solving a 1D lamination problem and incorporates it in the macro-model of the device at hand.

Our time-domain homogenisation methodology [36] can be clasified, regarding accuracy and computational complexity, in-between the multiscale computational approaches and the so-called pragmatic homogenisation referred to hereupon. Starting from the 1D eddy-current model of a lamination, dedicated skin-effect basis functions serve to interpolate the magnetic flux density, and the magnetic constitutive law is weakly imposed. The resulting system of equations is subsequently integrated into/coupled to the FE model of the considered application. It is applicable to saturable magntic cores and was validated on a real 3D test case (laminated ring core and toroidal coil, exploiting axisymmetry). Preliminary results with a hysteretic law were presented in [37]. The theoretical developments, detailed in the following sections, hold for any other available hysteresis models, see. e.g. [38]. As validation, we consider the following applications: 1) a toroidal stacked ring core of non-oriented steel sheets, including hysteresis; and 2) a 2D FE model of a switched reluctance motor considering the eddy-current effects and movement.

II. 1D model of a lamination

Our homogenisation approach is based on the 1D model of a ferromagnetic lamination; this frequency/time-domain model is hereafter embedded in a finite element implementation. Let us thus consider a lamination of thickness d ($-d/2 \leq z \leq d/2$), made of a homogeneous isotropic material with constant conduc-

tivity σ (resistivity $\rho = \sigma^{-1}$). We assume the magnetic flux density (or induction) $b(z,t)$ and magnetic field $h(z,t) = \nu\, b(z,t)$ along the x-axis; the electric current density $j(z,t)$ and electric field $e(z,t) = \rho\, j(z,t)$ along the y-axis. We adopt a linear electric constitutive law, $j = \sigma e$. The magnetic constitutive law $h = \mathcal{H}(b)$ can be nonlinear irreversible (hysteretic), nonlinear reversible or linear ($h = \nu b$, with constant reluctivity $\nu = \mu^{-1}$, permeability μ). The 1D eddy-current problem is governed by Ampere's and Faraday's 1D equations:

$$\partial_z h(z,t) = j(z,t)\,, \tag{1}$$
$$\partial_z e(z,t) = \partial_t b(z,t)\,, \tag{2}$$

and thus fully described by following partial differential equation (PDE):

$$\partial_z^2 h(z,t) = \sigma\, \partial_t b(z,t)\,. \tag{3}$$

We further define the quantities relevant to the homogenisation procedure, namely: 1) the magnetic flux density averaged over the lamination thickness $b_0(t) = \frac{1}{d}\int_{-d/2}^{d/2} b(z,t)\,\mathrm{d}z$; 2) the electric current density averaged over the lamination thickness $j_0(t) = \frac{1}{d}\int_{-d/2}^{d/2} j(z,t)\,\mathrm{d}z$; 3) the surface magnetic fields $h_\mathrm{s}^\pm(t) = h(\pm d/2, t)$ ($+$ and $-$ denote the upper and lower sides) and the average of these surface fields $h_\mathrm{s} = (h_\mathrm{s}^+ + h_\mathrm{s}^-)/2$; and 4) the surface electric fields $e_\mathrm{s}^\pm(t) = e(\pm d/2, t)$ and the associated average $e_\mathrm{s} = (e_\mathrm{s}^+ + e_\mathrm{s}^-)/2$.

The electromagnetic fields b, h, j and e exhibit symmetry with respect to the middle of the lamination, $z = 0$, so we distinguish two dual cases, that are simultaneously present in a lamination along two orthogonal directions (parallel directions, x and y, and stacking direction, z) [39, 10]. The *net-flux* case corresponds to imposing a nonzero net flux and a zero net current and verifies the following symmetries: $b(z,t) = b(-z,t)$, $h_\mathrm{s}^+ = h_\mathrm{s}^-$, $j(z,t) = -j(-z,t)$, $j_0 = 0$ and $e_\mathrm{s} = 0$. The *net-current* case corresponds to a nonzero net current and zero net flux with associated symmetries: $j(z,t) = j(-z,t)$, $e_\mathrm{s}^+ = e_\mathrm{s}^-$, $b(z,t) = -b(-z,t)$, $b_0 = 0$ and $h_\mathrm{s} = 0$, as depicted in Fig. 1.

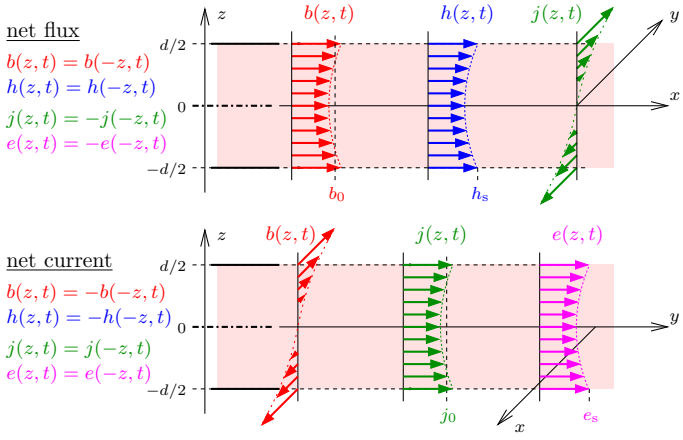

Fig. 1. 1D lamination model with local coordinate system xyz and with net flux along x (up) or net current along y (down) [31]

The closed-form analytical time-harmonic solution of (3) (complex quantities in bold, imaginary number $\boldsymbol{\jmath} = \sqrt{-1}$, frequency f and pulsation $\omega = 2\pi f$), yields a complex reluctivity $\boldsymbol{\nu}$ for the *net-flux* case and a complex resistivity $\boldsymbol{\rho}$ for the *net-current* case [13, 40]:

$$\boldsymbol{\nu} = \frac{\boldsymbol{h}_\mathrm{s}}{\boldsymbol{b}_0} = \nu\,\boldsymbol{\Gamma}\left(\frac{d}{\delta}\right) \quad \text{and} \quad \boldsymbol{\rho} = \frac{\boldsymbol{e}_\mathrm{s}}{\boldsymbol{j}_0} = \rho\,\boldsymbol{\Gamma}\left(\frac{d}{\delta}\right), \tag{4}$$

with $\boldsymbol{b}_0$ and $\boldsymbol{j}_0$ the average induction and current density, $\boldsymbol{h}_\mathrm{s}$ and $\boldsymbol{e}_\mathrm{s}$ the surface magnetic and electric field. The frequency dependence is contained in

$$\boldsymbol{\Gamma}\left(\frac{d}{\delta}\right) = \frac{1+\boldsymbol{\jmath}}{2}\,\frac{d}{\delta}\,\coth\left(\frac{1+\boldsymbol{\jmath}}{2}\,\frac{d}{\delta}\right), \tag{5}$$

with penetration depth $\delta = \sqrt{2/(\omega\mu\sigma)}$.

In the time domain, the governing PDE (3) can be solved by choosing suitable ansatzes for $b(z,t)$, $h(z,t)$ and $j(z,t)$ that minimize the spatial degrees of freedom in $-d/2 \le z \le d/2$. These fields are thus expanded in terms of *ad hoc* polynomial basis functions (BFs) $\alpha_k(z)$, $\beta_k(z)$ and $\gamma_k(z)$ of order k.

We have chosen as BFs for $b(z,t)$ the Legendre polynomials, $\alpha_k(z)$, which are mutually orthogonal, $(1/d)\int_{-d/2}^{d/2}\alpha_i\alpha_j\,\mathrm{d}z = 0$ if $i \neq j$, and have absolute value one at the lamination surface $|\alpha_i(\pm d/2)| = 1$. The expansion reads

$$b(z,t) = \sum_{k=0}^{n} \alpha_k(z)\, b_k(t)\,, \tag{6}$$

with $n \ge 0$ the order of the expansion. Other feasible choices can be found in the literature, e.g. a truncated Fourier cosine series in [41, 42] or the Gauss-Lobatto polynomials in [16].

In order to satisfy PDE (3), the expansion of the magnetic field $h(z,t)$ is given by

$$h(z,t) = h_\mathrm{s}(t)\; + j_0(t) z - \sum_{k=0}^{n} \sigma d^2\, \beta_{k+2}(z)\, \partial_t b_k\,, \tag{7}$$

in terms of the average surface magnetic field $h_\mathrm{s}(t)$, the average current density $j_0(t)$ and polynomials $\beta_{k+2}(z)$ that are null at the lamination surface $\beta_{k+2}(\pm d/2) = 0$ and verify $-d^2\partial_z^2\beta_{k+2}(z) = \alpha_k(z)$. Applying 1D Ampere's equation (1) to (7), we obtain the expansion of $j(z,t)$:

$$j(z,t) = j_0(t) - \sum_{k=0}^{n} \sigma d\, \gamma_{k+1}(z)\, \partial_t b_k\,, \tag{8}$$

with $\gamma_{k+1}(z) = d\,\partial_z\beta_{k+2}$. For the *net-flux* case, we can restrict the expansion to the even polynomials, i.e. α_k with even order k [36]; for the *net-current* case, we must add the odd polynomials, i.e. odd k [31]. The even polynomials α_k together with the associated β_k and γ_k are depicted in Fig. 2.

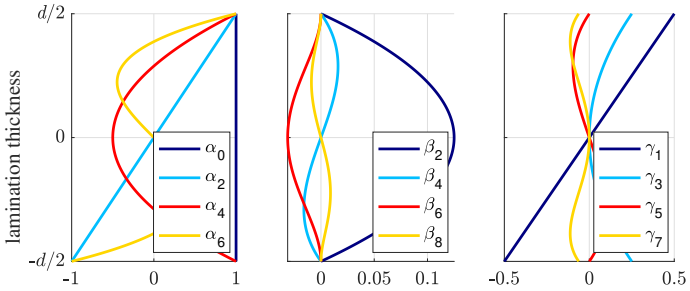

Fig. 2. From left to right: polynomial basis functions $\alpha_k(z)$, $\beta_k(z)$ and $\gamma_k(z)$ (of order k) used for expanding, respectively, $b(z,t)$, $h(z,t)$ and $j(z,t)$ along the lamination thickness $-d/2 \le z \le d/2$ in the net-flux case.

When considering a finite number of BFs, up to order n for $\alpha_k(z)$, order $n+2$ for $\beta_k(z)$, and order $n+1$ for $\gamma_k(z)$, the magnetic constitutive law $h = \mathcal{H}(b)$ cannot be satisfied. We derive the weak formulation of this material law by multiplying it with test functions, in a Galerkin approach equal to the BFs

of $b(z,t)$ (6), $\alpha_l(z)$ ($0 \le l \le n$), and integrating over the lamination thickness, i.e.

$$\frac{1}{d}\int_{-d/2}^{d/2}\Big(h(z,t)-\mathcal{H}(b(z,t)\Big)\,\alpha_l(z)\,\mathrm{d}z \;=\; 0\,, \qquad (9)$$

which leads to $n+1$ linear first-order ODEs in terms of the $n+1$ $b_k(t)$, where $h_\mathrm{s}(t)$ and $j_0(t)$ are a priori the given time-dependent source quantities.

In what follows, we restrict the theoretical developments to the pure *net-flux* case. Indeed, these are relevant for the finite element implementation with a hysteretic law that is addressed in this contribution and validated via two application examples. The combined *net-flux/net-current* case can be found in [31].

The discretisation of (9) with linear constitutive law $\mathcal{H}(b) = \nu_{fe}\,b$ leads to the system

$$\big[H_\mathrm{s}(t)\big] = \nu_{fe}\big[P(z)\big]\big[B(t)\big] + \sigma d^2\big[Q(z)\big]\partial_t\big[B(t)\big]\,, \qquad (10)$$

with $\big[H_\mathrm{s}(t)\big] = \big[h_\mathrm{s}(t)\;\;0\;\;\cdots\;\;0\big]^T$ and $\big[B(t)\big] = \big[b_0(t)\;b_2(t)\;\cdots\;b_n(t)\big]^T$. Given the orthogonality of the $\alpha_k(z)$, matrix $\big[P(z)\big]$ is diagonal. Moreover the $\beta_k(z)$ and the $\alpha_l(z)$ are also orthogonal unless $|k-l|$ equals 0 or 2, so matrix $\big[Q(z)\big]$ is tridiagonal. Their elements p_l and $q_{k,l}$ are given by

$$p_l = \frac{1}{d}\int_{-d/2}^{d/2}\alpha_l(z)^2\,\mathrm{d}z \;=\; \frac{1}{2l+1} \qquad (11)$$

$$q_{k,l} = \frac{1}{d}\int_{-d/2}^{d/2}\alpha_l(z)\,\beta_{k+2}(z)\,\mathrm{d}z\,. \qquad (12)$$

In the nonlinear case, with either reversible or hysteretic constitutive law, we have

$$\big[H_\mathrm{s}(t)\big] = \int_{-d/2}^{d/2}\mathcal{H}\big(b(z,t)\big)\big[A(z)\big]\mathrm{d}z \;+\sigma d^2\big[Q(z)\big]\partial_t\big[B(t)\big] \qquad (13)$$

with $b(z,t)$ given by the expansion (6) and $[A(z)] = [\alpha_0(z)\;\alpha_2(z)\;\cdots\;\alpha_n(z)]^T$.

The time derivative in systems (10) and (13) is discretised by an implicit $\theta-$method, $0.5 \le \theta \le 1$, including backward Euler ($\theta = 1$) or Crank-Nicolson scheme ($\theta = 0.5$), obtaining a system of linear/nonlinear algebraic equations for each time step from t_i to $t_{i+1} = t_i + \Delta t$. In case of nonlinearity, the Newton-Raphson method is applied at each time step. With given $h_\mathrm{s}(t)$, the Jacobian matrix reads

$$\frac{\theta}{d}\int_{-d/2}^{d/2}\frac{\mathrm{d}\mathcal{H}}{\mathrm{d}b}\big[\Lambda(z)\big]\,\mathrm{d}z + \frac{\sigma d^2}{\Delta t}\,\big[Q(z)\big]\,, \qquad (14)$$

where $\dfrac{\mathrm{d}\mathcal{H}}{\mathrm{d}b}$ is the differential reluctivity and the matrix $[\Lambda(z)]$ has elements $\lambda_{k,l} = \alpha_k(z)\,\alpha_l(z)$ with $k,l = 0,2,\ldots,n$.

For a prescribed maximum error, the order n of the spatial interpolation of $b(z,t)$ must be increased along with the frequency f (or the relative lamination thickness d/δ). The integration in the lamination thickness can be done numerically (Gauss quadrature) and limited to interval $[0, d/2]$, exploiting symmetry with respect to $z = 0$. For hysteretic material models, the differential reluctivity tensor also depends on the history of the material. At the FE implementation level, this history has to be kept at level of the Gauss points used in the 1D lamination model. Any hysteresis model could be embedded in the 1D system (13), classical e.g. the Preisach model [43], the Jiles-Atherton model [44, 45] or more recent ones like the Energy-consistent hysteresis model [46] or the so-called G hysteresis model [47].

III. Homogenisation in a finite element model

We consider a magnetodynamic problem in a bounded domain $\Omega \in \mathbb{R}^3$. The problem is formulated in terms of the (modified) magnetic vector potential, $\underline{a}$, as

$$\mathrm{curl}\,\underline{\mathcal{H}}\,(\underline{b}) + \sigma\partial_t\underline{a} = \underline{j}_s\,, \qquad (15)$$

with $\underline{h} = \underline{\mathcal{H}}\,(\underline{b})$ the magnetic field characterised by the material law $\underline{\mathcal{H}}$ (linear or not), $\underline{j}_s$ the imposed source current density, the magnetic flux density $\underline{b} = \mathrm{curl}\,\underline{a}$ and the induced current density $\underline{j} = -\sigma\partial_t\underline{a}$. Underlined symbols indicate vector quantities. In the interest of clarity, we assume that only the laminated iron core $\Omega_\ell \in \Omega$ is conducting and may be nonlinear (i.e. the constitutive law outside Ω_ℓ is $\underline{h} = \nu\underline{b}$, linear and isotropic); the insulating layers have a negligible thickness (fill factor ≈ 1); and that $\underline{\mathcal{H}}$ and $\underline{b}$ are parallel to the plane of the laminations. Ampere's law (15) in weak form reads: find $\underline{a}$ so that

$$\begin{aligned}(j_s, \underline{a}')_{\Omega_s} = {}& (\nu\,\mathrm{curl}\,\underline{a}, \mathrm{curl}\,\underline{a}')_{\Omega\setminus\Omega_\ell} \\ & + (\underline{\mathcal{H}}(\underline{b}), \mathrm{curl}\,\underline{a}')_{\Omega_\ell} + (\sigma\,\partial_t\underline{a}, \underline{a}')_{\Omega_\ell}\,, \end{aligned} \qquad (16)$$

holds for all weighing function $\underline{a}'$ in a suitable function space and with suitable boundary conditions. $(\cdot,\cdot)_\Omega$ denotes a volume integral in Ω of the scalar product of its arguments. $\underline{a}$ is discretised by e.g. standard edge elements (3D domain or 2D domain with in-plane current density) with a tree-cotree gauge condition in Ω/Ω_ℓ, the non-conducting part of Ω [36]. This reference $\underline{a}-$formulation (16) requires the explicit modelling of each lamination and a sufficiently fine mesh in the thickness direction.

Hereafter, we detail the homogenisation approach that consists in embedding the previously described 1D lamination model in the FE formulation (16). The so-called homogenised formulation allows for a coarse discretisation of the lamination stack, with a mesh that is independent of the lamination thickness and orientation. The coupling is naturally done via $\mathrm{curl}\,\underline{a}$, as the first component of the expansion (6) is associated to a constant BF, $\alpha_0 = 1$, and defined as the average flux density. We thus adopt $\underline{b}_0 = \mathrm{curl}\,\underline{a}$ in the laminated domain Ω_ℓ. The homogenised weak form reads: find $\underline{a}$ and $\underline{b}_k$, $k = 0, 2, \ldots, n$ so that

$$\begin{aligned}\Big(\underline{j}_s, \underline{a}'\Big)_{\Omega_s} = {}& (\nu\,\mathrm{curl}\,\underline{a}, \mathrm{curl}\,\underline{a}')_{\Omega\setminus\Omega_\ell} \\ & + (\underline{\mathcal{H}}^z, \mathrm{curl}\,\underline{a}')_{\Omega_\ell} + \sum_{k\le 2}\big(\sigma d^2 q_{k,0}\,\partial_t\underline{b}_k, \mathrm{curl}\,\underline{a}'\big)_{\Omega_\ell}\,, \\ & \big(\underline{\mathcal{H}}^z, \underline{b}_l'\big)_{\Omega_\ell} + \sum_k\big(\sigma d^2 q_{k,l}\,\partial_t\underline{b}_k, \underline{b}_l'\big)_{\Omega_\ell} = 0\,, \end{aligned} \qquad (17)$$

holds for all weighing function $\underline{a}'$ and $\underline{b}_l'$, $l = 2,\ldots,n$ and $n > 0$ in a suitable function space and with appropriate boundary conditions. The additional $\underline{b}_k$, $k = 2,\ldots,n$ in Ω_ℓ are discretised by e.g. standard facet elements. Alternatively, one may define additional $\underline{a}_k$ such that $\underline{b}_k = \mathrm{curl}\,\underline{a}_k$ and use edge elements as for $\underline{a}$. The coefficients $q_{k,l}$ can be precalculated using (12). The function $\underline{\mathcal{H}}^z$ denotes the integration of the material law along the thickness of the lamination in terms of all the induction components $(\underline{b}_0, \cdots, \underline{b}_n)$:

$$\underline{\mathcal{H}}^z\,(\underline{b}_0, \cdots, \underline{b}_n) = \frac{1}{d}\int_{-d/2}^{d/2}\underline{\mathcal{H}}\left(\sum_k \alpha_k(z)\underline{b}_k\right)\,\alpha_l(z)\,\mathrm{d}z\,, \qquad (18)$$

with $k,l = 0,2,\ldots,n$.

Note that in the linear case, the integral (18) simplifies to

$$\underline{\mathcal{H}}^z\,(\underline{b}_0, \cdots, \underline{b}_n) = \sum_k \nu_{fe}\,p_k\,\underline{b}_k\,, \quad k = 0,2,\ldots,n \qquad (19)$$

with p_k from (11).

The system of nonlinear algebraic equations obtained after space and time discretization of (17) can be solved by means of the Newton-Raphson method. The contribution of Ω_ℓ to the elements of the Jacobian matrix is determined by the differential reluctivity tensor $\dfrac{\partial \underline{\mathcal{H}}^z}{\partial \underline{b}}$, i.e. deriving the equations with regard to the unknowns $(\underline{b}_0, \cdots, \underline{b}_n)$. This tensor is directly linked to (14) and accounts for the integration along the lamination thickness.

For hysteretic material models, $\underline{\mathcal{H}}$ in (18) is replaced by a given hysteretic law $\underline{\mathcal{H}}^h$ (e.g. Preisach, Jiles-Atherton, Energy-consistent, etc.) that requires the present state $(\underline{b}, \underline{h})$ of the material as well as its history:

$$\underline{\mathcal{H}} = \underline{\mathcal{H}}^h \left(\sum_k \alpha_k(z) \underline{b}_k \, , \underline{h}, \text{history} \right) , \tag{20}$$

which implies keeping track of the additional unknowns $\underline{b}_k$ at previous instants and per Gauss integration point through the lamination thickness. The discretised system is then solved by applying the Newton-Raphson scheme per time step.

IV. Numerical simulations

Hereafter we consider two relevant applications: 1) a toroidal stacked ring core of non-oriented steel sheets that highlights the validity of the homogenisation approach with a hysteresis law; 2) a 2D FE model of a switched reluctance motor accounting for the eddy-current effects at high frequency and high imposed speed that successfully prevents a cumbersome 3D counterpart.

All theoretical developments have been implemented within the open-source FE software bundle ONELAB [48], that comprises the mesh generator Gmsh [49] and the FE solver GetDP [50]. The files used to perform the simulations are available on demand and soon at `https://gitlab.onelab.info/doc/models/-/wikis/home`.

A. A stacked ring core

As first validation test case, we study a stacked ring core surrounded by an inductor. Neglecting curvature (1 m along z), the model is two-dimensional with in-plane induced currents (on xy-plane) and out of plane flux density. The core comprises 2×10 laminations (thickness $d = 0.5\,\text{mm}$, $\sigma = 2\,\text{MS/m}$) separated by horizontal insulation layers (thickness $d_i = 0.05\,\text{mm}$, non-conducting $\sigma = 0$ and non-magnetic $\mu_r = 1$). The FeSi steel laminations are characterised by a vector Jiles-Atherton (JA) model [45] with parameters $m_s = 1145220\text{A/m}$, $a = 59.5\,\text{A/m}$, $k = 99.2\,\text{A/m}$, $c = 0.54$ and $\alpha = 1.3\,10^{-4}$.

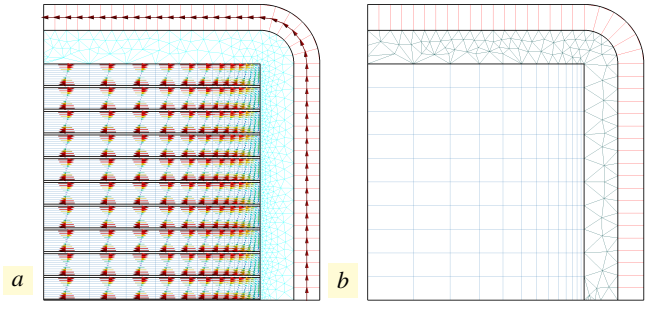

Fig. 3. 2D FE model of stacked ring core, coil and air in-between (1/4 cross-section). a) fine reference mesh with in-plane imposed and induced current density (2 kHz, real part); b) mesh of homogenised core.

In the brute-force fine reference model (Fig. 3, a) each half lamination cross-section is split up in 13×10 quadrangles, separated by a single layer of quadrangles (insulation), for a total of 7657 real-valued unknowns associated to edges (after gauging). The homogenised lamination stack (including the insulation) is split up in 13×10 quadrangles (Fig. 3, b), with 130 additional unknowns (associated to the quadrangles) per $\underline{b}_l$ ($l = 2, 4, \ldots, n$), on top of the 764 unknowns (associated to edges) when $n = 0$. The fill factor of the laminated core, $\lambda = 50/55 = 90.1\%$, is simply accounted for by decreasing conductivity, i.e. $\lambda\sigma$, and increasing reluctivity, i.e. ν/λ or increasing $\underline{b}$ in the JA hysteretic law $\underline{\mathcal{H}}^h(\underline{b}/\lambda)$ [51, 52, 10].

We impose a time-varying sinusoidal source current density $\underline{j}_s$ in the coil (Ω_s, outer layer of quadrangles) with same amplitude and frequencies in the range $[5, 5000]$ Hz. Time-stepping simulations are performed using backward Euler with 240 steps per period and starting from the zero solution.

The flux linkage versus imposed current at $50, 500$ and $5000\,\text{Hz}$ is shown in Figs. 4. The effect of the eddy currents with the increasing frequency is evident in these global hysteresis loci. A good convergence of the homogenised cases ($n = 0, 2, 4$) towards the reference results ("ref.") is observed for all considered frequencies. The higher the frequency, the more additional basis functions (higher n) are required for an accurate homogenisation. This behaviour is also observed in Fig. 5 that depicts the flux linkage versus time (normalised time for a period in steady state) for the same set of frequencies: $n = 0$ provides a perfect fit at 50 Hz; $n = 2$ and $n = 4$ give an excellent agreement at 500 and and 5000 Hz, respectively.

The overall losses per cycle computed by the homogenised model with $n = 0, 2, 4$ are compared with those obtained with the reference fine model in Fig. 6 for $f \in [5, 5000]$ Hz. These losses are the area of the loci (flux vs. current) shown in Fig. 4. Note that these curves include eddy current and hysteresis effects. The pure hysteretic losses may be determined by substracting the losses obtained when using the corresponding anhysteretic magnetisation curve (average of the ascending and descending branches of the major hysteresis loop). The higher the frequency, the higher the value of n must be for ensuring accuracy.

For 240 time steps, the computation time on a MacBook Pro 2.9GHz Quad-core Intel i7 (average number of NR iterations per step indicated between parentheses) is approximately 84 s (5) with the fine reference mesh, and 3.6 s (3), 11.2 s (4) and 16.7 s (5) with homogenisation and n equal to 0, 2 and 4, with no noticeable dependence on the frequency.

B. Switched reluctance motor

We consider now a switched reluctance motor (SRM), the geometry and main dimensions of which are provided in Fig. 7. The homogenisation approach is here embedded within a 2D FE model of the machine and validated with its fine 3D magnetodynamic counterpart, considering one lamination (thickness $d = 0.5\,\text{mm}$, conductivity $\sigma = 5\,\text{MS/m}$) and the eddy-current distribution. Preliminary results were presented in [53]. Both models are based on an $\underline{a}$-formulation with edge unknowns for $\underline{a}$ in 3D and nodal unknowns for the $z-$component of $\underline{a}$, a_z, in 2D. The additional homogenisation unknown fields $\underline{b}_k, k = 2, 4, \ldots, n$ in 2D are discretised by means of a $90°$ rotation of classical edge basis functions. A nonlinear BH relation is considered for the laminations, viz. $\nu = h/b = 100 + 10e^{1.8b^2}$ with h in A/m and b in T.

Symmetry considerations allow modelling half cross-section of

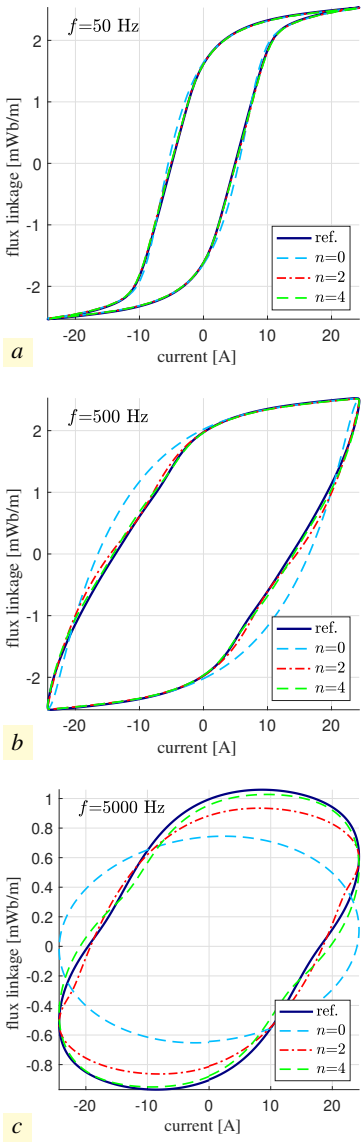

Fig. 4. Flux linkage versus imposed sinusoidal current (amplitude $I = 25$ A) obtained with the fine reference and coarse homogenised models ($n = 0, 2, 4$) at a) 50 Hz; b) 500 Hz; and c) 5000 Hz.

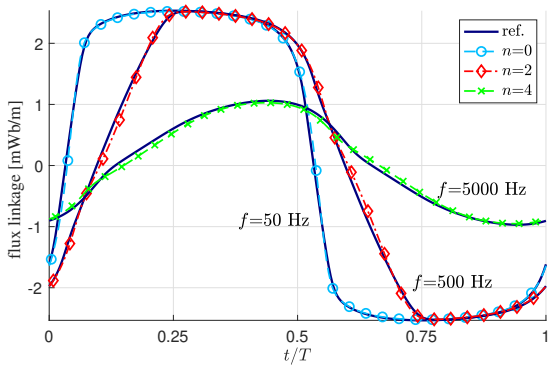

Fig. 5. Flux linkage versus normalised time (one period in steady state) obtained with the fine reference and coarse homogenised models ($n = 0, 2, 4$) at 50, 500 and 5000 Hz.

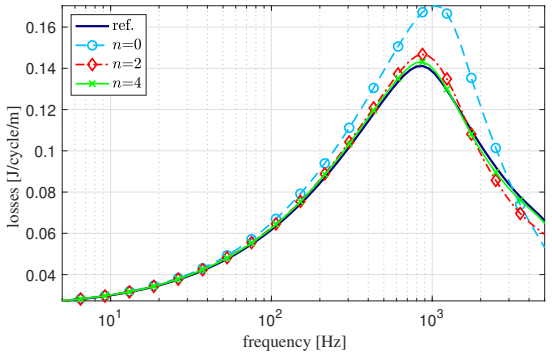

Fig. 6. Losses per cycle in laminated core as a function of frequency obtained with the reference and homogenised model ($n = 0, 2, 4$).

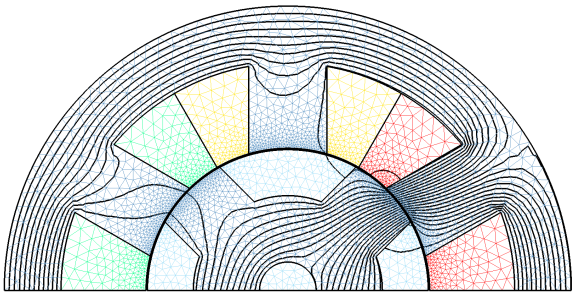

Fig. 7. Half cross-section of 6/4 SRM (airgap radius: 30 mm; airgap width: 0.29 mm; stack length: 60 mm; lamination thickness d: 0.5 mm; stator and rotor pole width: 16 mm; outer radius: 60 mm; 226 turns per coil) – flux lines with phase 1 (red) excited and 15° misalignment.

the machine in 2D and extruding this domain over half a lamination thickness in 3D ($0 \leq z \leq d/2$). The position angle 0° corresponds to the perfect alignment of rotor poles with the stator poles of phase 1 (in red in Fig. 7). The 2D mesh ccomprises 6253 triangles and 360 quadrangles, 180 quadrangles on the rotor and stator layer bands touching the corresponding sliding surfaces for handling the rotation [54]. This discretisation gives rise to 3477 nodal unknowns with $n = 0$, plus 5718 perpendicular facet unknowns when increasing n, i.e. a total of 9195 unknowns with $n = 2$ and 14913 unknowns with $n = 4$. The 3D mesh is created by extruding the 2D mesh with 5 layers of elements in geometrical progression (common ratio $r = 0.5$), yielding 31265 prisms and 1800 hexahedra in the sliding-surface bands. See Figs. 8 for a detail of the 3D mesh. The number of (complex- or real-valued) edge unknowns associated to this mesh is 41954.

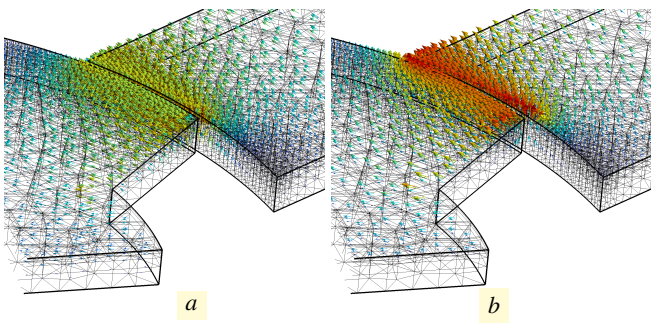

Fig. 8. Current density at standstill with phase 1 excited at $f = 5$ kHz, 3D FE model of half lamination. Detail of the mesh (thickness scaled by a factor 10 for the sake of visibility). Components a) in phase and b) in quadrature with imposed current.

Dynamic frequency-domain calculations are first carried out imposing a unit-amplitude sinusoidal current in the phase 1 with

the frequency ranging from 10 Hz to 10 kHz. By way of illustration, the current density in half a lamination obtained with the 3D reference model at standstill and a $f = 5$ Hz-sinusoidal imposed current is represented in Fig. 8 (lamination thickness scaled by a factor 10 to enhance visibility, 15° misalignment between rotor and stator poles). The eddy-current loss distribution obtained with the 2D homogenised model and the analytical complex reluctivity (4) is shown as well in Fig. 9.

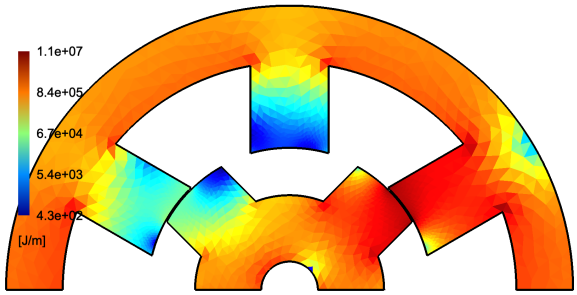

Fig. 9. Eddy-current loss distribution with phase 1 excited at $f = 5$ kHz, obtained with the frequency-domain 2D homogenised model and the analytical complex reluctivity. The rotor and stator teeth are misaligned, 15°, standstill.

Fig. 10 represents the complex inductance obtained with the 3D reference model, the 2D models with analytical complex reluctivity (4) ("2D ana."), and with $n = 0, 2, 4$ for the cases with fully aligned and misaligned rotor/stator poles. The 2D analytical and $n = 4$ models and produces very accurate results in the complete frequency interval. The 2D $n = 2$ model guarantees this level of accuracy up to 3 kHz and 4 kHz for the aligned and misaligned cases. With $n = 0$, the accuracy is still high up to 300 Hz and 700 Hz for the aligned and misaligned positions.

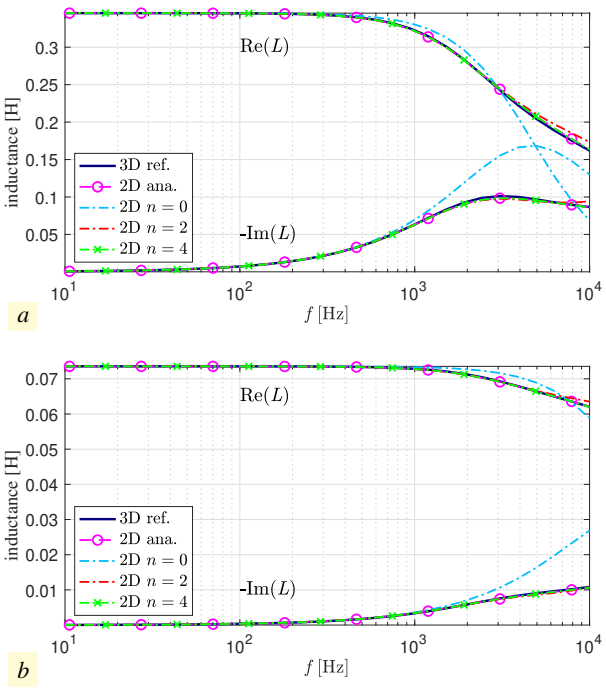

Fig. 10. Inductance (real and imaginary part) versus frequency obtained with the reference 3D FE model and the 2D homogenised FE model ($n = 0, 2, 4$). Stator and rotor teeth a) at 0°, fully aligned; b) at 30°, fully misaligned.

Time-stepping simulations are performed for a 2 kHz, ±300 V pulsed voltage supply, that depends on the rotor position, and with imposed speed of 20000 rpm. We adopt a fixed step of 0.5°, i.e. $\Delta t = 0.33\,\mu$s. The flux linkage and current of the phase that is activated first as well as the torque versus time are depicted in Fig. 11 for the first 0.75 ms (corresponding to a rotation of 90°). The results obtained with the 2D homogenised model $n = 0, 2, 4$ agree very well with those given by the 3D reference computation, only small deviations are visible to the naked eye with $n = 0$. A zoom on the flux (Fig.11 a) allows to observe the convergence of the curves with increasing order. In the same time range, we have also computed the eddy-current losses in rotor and stator, that are represented in Fig. 12. One observes a clear and satisfactory convergence of the results, with an excellent accuracy for $n = 4$, accuracy which is already very high for $n = 2$. With $n = 0$, the losses are grossly overestimated.

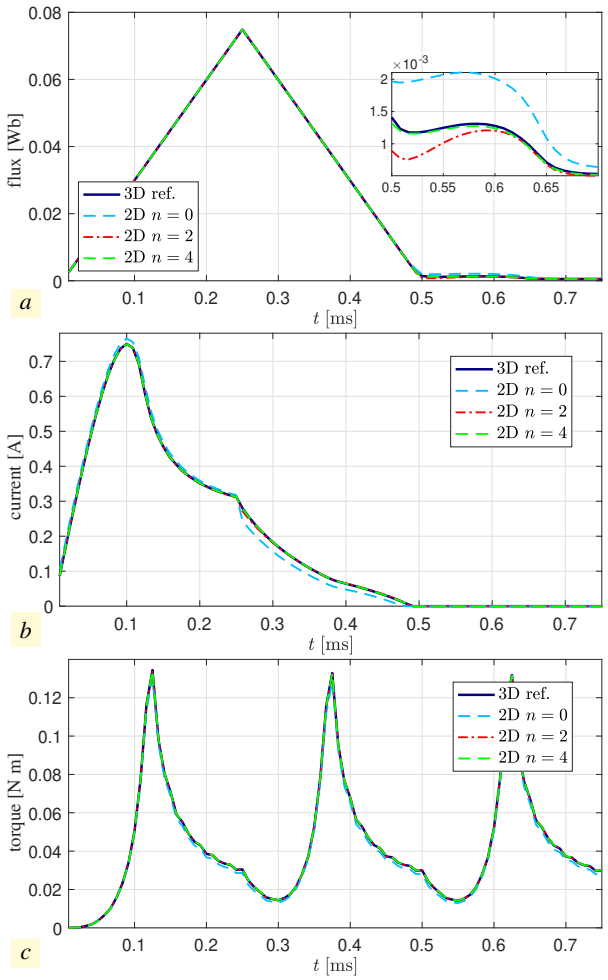

Fig. 11. $f = 2$ kHz, ±300 V PWM voltage and imposed speed of 20000 rpm: a) linkage flux (zoom with $t \in [0.5, 0.7]$ s); b) current; and c) torque versus time btained with the reference 3D FE model and the 2D homogenised FE model ($n = 0, 2, 4$).

By way of illustration, we provide hereafter the CPU time for 360 steps on a MacBook Pro 2.9GHz Quad-core Intel i7. For the 3D reference model, the CPU time is 2526 s, while for the 2D homogenised model the CPU time amounts to 62 s, 355 s and 797 s with $n = 0, 2, 4$, respectively. The average number of NR iterations per time step in all cases is 3.

V. Conclusions and Perspectives

Herein we have provided an overview of the available homogenisation techniques applied to laminated cores with eddy currents in computational electromagnetics. We have further focused on the development of the theory for magneto-quasi-static problems in the time domain, including a hysteresis material law. Two real-life applications have served as validation: a laminated core with hysteretic material and a rotating machine with

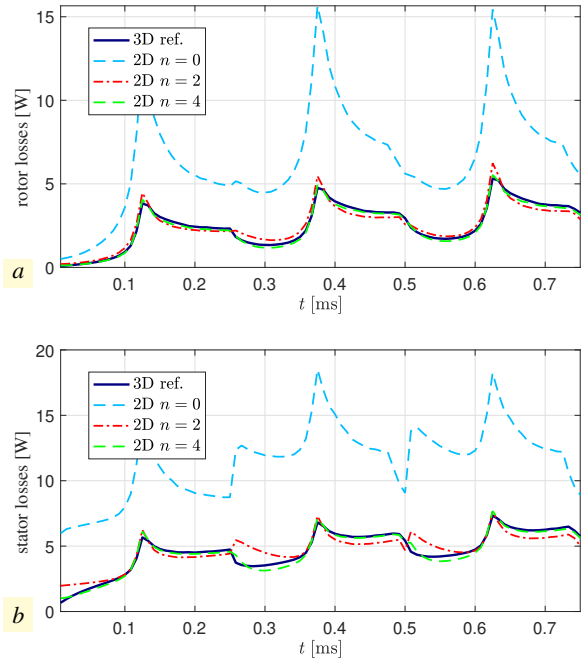

Fig. 12. Eddy-current losses versus time obtained with the reference 3D FE model and the 2D homogenised FE model ($n = 0, 2, 4$). a) in the rotor; b) in the stator. $f = 2\,\text{kHz}$ PWM voltage, 20000 rpm imposed speed

eddy currents in stator and rotor. The homogenisation approach has proved to be highly accurate and efficient, and therefore a feasible alternative to brute-force finite element models.

In spite of the huge amount of efforts and successful developments that have been reported in the literature, the modelling of losses of ferromagnetic laminated structures is still nowadays an open problem as evidenced by the numerous recent contributions, the very latest, this year. Homogenisation techniques are tainted by errors inherent to their underlying assumptions (periodicity, asymptotic behaviour, etc.), edge effects are indeed neglected. Therefore, the analysis of laminated steel in the presence of non negligible perpendicular flux remains a challenge. The fringing fields cause flux redistribution in the individual sheets due to saturation and generate even more perpendicular flux that affects the adjacent laminations [55], to what extent is not known *a priori*. Adopting hybrid models, that combine homogenisation with localised standard 2D or 3D FE models of one or more outer laminations, may provide a proper compromise between efficiency and accuracy [56, 29, 57]. A thorough analysis of this kind of domain decomposition/subproblem approach, including sensitivity, is still missing and needed for the sake of robustness.

References

[1] K. R. Geldhof, A. Van den Bossche, and J. A. A. Melkebeek, "Influence of eddy currents on resonance-based position estimation of switched reluctance drives," in *International Conference on Electrical Machines and Systems, Wuhan, China, October 17-20*, 2008, pp. 2820–2825.

[2] G. Bertotti, A. Boglietti, M. Chiampi, D. Chiarabaglio, F. Fiorillo, and M. Lazzari, "An improved estimation of iron losses in rotating electrical machines," *IEEE Trans. Magn.*, vol. 27, no. 6, pp. 5007–5009, 1991.

[3] D. M. Ionel, M. Popescu, M. I. McGilp, T. J. E. Miller, S. J. Dellinger, and R. J. Heideman, "Computation of core losses in electrical machines using improved models for laminated steel," *IEEE Trans. Ind. Appl.*, vol. 43, no. 6, pp. 1554–1564, 2007.

[4] V. C. Silva, G. Meunier, and A. Foggia, "A 3D finite element computation of eddy currents and losses in laminated iron cores allowing for electric and magnetic anisotropy," *IEEE Trans. Magn.*, vol. 31, no. 3, pp. 2139–2141, 2005.

[5] K. Preis, O. Bíró, and I. Ticar, "FEM analysis of eddy current losses in nonlinear laminated iron cores," *IEEE Trans. Magn.*, vol. 41, no. 5, pp. 1412–1415, 2005.

[6] H. Kaimori, A. Kameari, and K. Fujiwara, "FEM computation of magnetic field and iron loss in laminated iron core using homogenization method," *IEEE Trans. Magn.*, vol. 43, no. 4, pp. 1405–1408, 2007.

[7] F. Martin, A. Belahcen, A. Lehikoinen, and P. Rasilo, "Homogenization technique for axially laminated rotors of synchronous reluctance machines," *IEEE Trans. Magn.*, vol. 51, no. 12, pp. 1–6, 2015.

[8] O. Bottauscio and M. Chiampi, "Analysis of laminated cores through a directly coupled 2-D/1-D electromagnetic field formulation," *IEEE Trans. Magn.*, vol. 38, no. 5, pp. 2358–2360, 2002.

[9] H. Igarashi, K. Watanabe, and A. Kost, "A reduced model for finite element analysis of steel laminations," *IEEE Trans. Magn.*, vol. 42, no. 4, pp. 739–742, 2006.

[10] H. De Gersem, S. Vanaverbeke, and G. Samaey, "Three-dimensional–two-dimensional coupled model for eddy currents in laminated iron cores," *IEEE Trans. Magn.*, vol. 48, no. 2, pp. 815–818, 2012.

[11] A. J. Bergqvist and S. G. Engdahl, "A homogenization procedure of field quantities in laminated electric steel," *IEEE Trans. Magn.*, vol. 37, no. 5, pp. 3329–3331, 2001.

[12] P. Dular, J. Gyselinck, C. Geuzaine, N. Sadowski, and J. P. A. Bastos, "A 3-D magnetic vector potential formulation taking eddy currents in lamination stacks into account," *IEEE Trans. Magn.*, vol. 39, no. 3, pp. 1424–1427, 2003.

[13] L. Krähenbühl, P. Dular, T. Zeidan, and F. Buret, "Homogenization of lamination stacks in linear magnetodynamics," *IEEE Trans. Magn.*, vol. 40, no. 2, pp. 912–915, 2004.

[14] I. Niyonzima, R. V. Sabariego, P. Dular, F. Henrotte, and C. Geuzaine, "Computational homogenization for laminated ferromagnetic cores in magnetodynamics," *IEEE Trans. Magn.*, vol. 49, no. 5, pp. 2049–2052, 2013.

[15] I. Niyonzima, R. V. Sabariego, P. Dular, K. Jacques, and C. Geuzaine, "Multiscale finite element modeling of nonlinear magnetoquasistatic problems using magnetic induction conforming formulations," *SIAM Multiscale Modeling and Simulation*, vol. 16, no. 1, pp. 300–326, 2018.

[16] M. Schöbinger, J. Schöberl, and K. Hollaus, "Multiscale FEM for the linear 2-D/1-D problem of eddy currents in thin iron sheets," *IEEE Trans. Magn.*, vol. 55, no. 1, pp. 1–12, 2019.

[17] M. Schöbinger, K. Hollaus, and I. Tsukerman, "Nonasymptotic homogenization of laminated magnetic cores," *IEEE Trans. Magn.*, vol. 56, no. 2, pp. 1–4, 2020.

[18] S. Ziani, T. Henneron, and Y. Le Menach, "Nonlinear lamination stacks studied with harmonic balance FEM supplied by magnetic flux arising from PWM," in *2016 IEEE Conference on Electromagnetic Field Computation (CEFC)*, 2016, pp. 1–1.

[19] R. V. Sabariego and J. Gyselinck, "Nonlinear harmonic-balance finite-element homogenisation of lamination stacks with net circulating currents," in *Proceedings of the 18th Biennial IEEE Conference on Electromagnetic Field Computation (CEFC2018)*, Hangzhou, Zhejiang, China, October 23–28, 2018.

[20] Y. Shindo, T. Miyazaki, and T. Matsuo, "Cauer circuit representation of the homogenized eddy-current field based on the legendre expansion for a magnetic sheet," *IEEE Trans. Magn.*, vol. 52, no. 3, pp. 1–4, 2016.

[21] Y. Sato, T. Shimotani, and H. Igarashi, "Synthesis of cauer-equivalent circuit based on model order reduction considering nonlinear magnetic property," *IEEE Trans. Magn.*, vol. 53, no. 6, pp. 1–4, 2017.

[22] M. Gołębiowski, L. Gołębiowski, A. Smoleń, and D. Mazur, "Direct consideration of eddy current losses in laminated magnetic cores in finite element method (FEM) calculations using the laplace transform," *Energies*, vol. 13, no. 5, p. 1174, Mar 2020.

[23] K. Hollaus, J. Schöberl, and M. Schöbinger, "MSFEM and MOR to minimize the computational costs of nonlinear eddy-current problems in laminated iron cores," *IEEE Trans. Magn.*, vol. 56, no. 2, pp. 1–4, 2020.

[24] S. B. Shah, P. Rasilo, A. Belahcen, and A. Arkkio, "Modeling of losses due to inter-laminar short-circuit currents in lamination stacks," *Electrical, Control and Communication Engineering*, vol. 3, no. 1, pp. 31–36, 2013.

[25] H. Hamzehbahmani, P. Anderson, K. Jenkins, and M. Lindenmo, "Experimental study on inter-laminar short-circuit faults at random positions in laminated magnetic cores," *IET Electr. Power Appl.*, vol. 10, no. 7, pp. 604–613, 2016.

[26] J.-Y. Roger, E. Vrignaud, T. Henneron, A. Benabou, and J. Ducreux, "Electromagnetic modelling of short circuited coreplates," *COMPEL - The international journal for computation and mathematics in electrical and electronic engineering*, vol. 28, no. 3, pp. 762–771, 2009.

[27] S. Ziani, T. Henneron, O. Puigdellivol, and Y. L. Menach, "A method coupling modified vector potential a* and homogenization formulations to model short-circuits in lamination stacks," *Eur. Phys. J. Appl. Phys.*, vol. 75, no. 3, pp. 1–8, Art. no. 30 901, 2016.

[28] H. Wang and Y. Zhang, "Modeling of eddy-current losses of welded laminated electrical steels," *IEEE Trans. Ind. Electron.*, vol. 64, no. 4, pp. 2992–3000, 2017.

[29] P. Dular, M. V. Ferreira da Luz, P. Kuo-Peng, and L. Krähenbühl, "Correction of homogenized lamination stacks via a subproblem finite element method," *COMPEL - The international journal for computation and mathematics in electrical and electronic engineering*, vol. 34, no. 5, pp. 1553–1563, 2015.

[30] P. Handgruber, A. Stermecki, O. Bíró, and G. Ofnery, "Evaluation of interlaminar eddy currents in induction machines," in *IECON 2013 - 39th Annual Conference of the IEEE Industrial Electronics Society*, 2013, pp. 2792–2797.

[31] J. Gyselinck, P. Dular, L. Krähenbühl, and R. V. Sabariego, "Finite-element homogenisation of laminated iron cores with inclusion of net circulating currents due to imperfect insulation," *IEEE Trans. Magn.*, vol. 52, no. 3, p. Art. no. 7209104, 2016.

[32] R. V. Sabariego, J. Gyselinck, Y. L. Menach, and T. Henneron, "Accuracy of homogenization techniques to model lamination stacks with interlaminar currents," in *Proceedings of the 22nd Conference on the Computation of Electromagnetic Fields (COMPUMAG2019)*, Paris, France, July 15–19, 2019.

[33] J. Pippuri and A. Arkkio, "Time-harmonic induction-machine model including hysteresis and eddy currents in steel laminations," *IEEE Trans. Magn.*, vol. 45, no. 7, pp. 2981–2989, 2009.

[34] F. Henrotte, S. Steentjes, K. Hameyer, and C. Geuzaine, "Pragmatic two-step homogenisation technique for ferromagnetic laminated cores," *IET Science, Measurement Technology*, vol. 9, no. 2, pp. 152–159, 2015.

[35] M. Schöbinger, S. Steentjes, J. Schöberl, K. Hameyer, and K. Hollaus, "MSFEM for the eddy current problem in a laminated core including hysteresis," *IEEE Trans. Magn.*, vol. 55, no. 8, pp. 1–9, 2019.

[36] J. Gyselinck, R. V. Sabariego, and P. Dular, "A nonlinear time-domain homogenization technique for laminated iron cores in three-dimensional finite element models," *IEEE Trans. Magn.*, vol. 42, no. 4, pp. 763–766, 2006.

[37] R. V. Sabariego, I. Niyonzima, C. Geuzaine, and J. Gyselinck, "Time-domain finite-element modelling of laminated iron cores – Large skin effect homogenization considering the Jiles-Atherton hysteresis model," in *Proceedings of the 15th Biennial IEEE Conference on Electromagnetic Field Computation (CEFC2012)*, Oita, Japan, November 11–14, 2012.

[38] S. Steentjes, K. Hameyer, D. Dolinar, and M. Petrun, "Iron-loss and magnetic hysteresis under arbitrary waveforms in no electrical steel: A comparative study of hysteresis models," *IEEE Trans. Ind. Electron.*, vol. 64, no. 3, pp. 2511–2521, 2017.

[39] P. Dular, J. Gyselinck, T. Zeidan, and L. Krähenbühl, "Finite element modelling of stacked thin regions with non-zero global currents," *COMPEL - The international journal for computation and mathematics in electrical and electronic engineering*, vol. 23, no. 3, pp. 707–714, 2004.

[40] O. Moreau, R. Michel, T. Chevalier, G. Meunier, M. Joan, and J. B. Delcroix, "3-D high frequency computation of transformer R, L parameters," *IEEE Trans. Magn.*, vol. 41, no. 5, pp. 1364–1367, 2005.

[41] P. Rasilo, E. Dlala, K. Fonteyn, J. Pippuri, A. Belahcen, and A. Arkkio, "Model of laminated ferromagnetic cores for loss prediction in electrical machines," *IET Electr. Power Appl.*, vol. 5, no. 7, pp. 580–588, 2011.

[42] C. Krüttgen, S. Steentjes, G. Glehn, and K. Hameyer, "Parametric homogenized model for inclusion of eddy currents and hysteresis in 2-D finite-element simulation of electrical machines," *IEEE Trans. Magn.*, vol. 53, no. 6, pp. 1–4, 2017.

[43] J. Gyselinck, L. Dupré, L. Vandevelde, and J. Melkebeek, "Calculation of no-load induction motor core losses using the rate-dependent preisach model," *IEEE Trans. Magn.*, vol. 34, no. 6, pp. 3876–3881, 1998.

[44] A. Bergqvist, "A simple vector generalisation of the Jiles-Atherton model of hysteresis," *IEEE Trans. Magn.*, vol. 32, no. 5, pp. 4213–4215, 1996.

[45] J. Gyselinck, P. Dular, N. Sadowski, J. Leite, and J. P. A. Bastos, "Incorporation of a Jiles-Atherton vector hysteresis model in 2D FE magnetic field computations," *COMPEL - The international journal for computation and mathematics in electrical and electronic engineering*, vol. 23, no. 3, pp. 685–693, 2004.

[46] K. Jacques, R. V. Sabariego, C. Geuzaine, and J. Gyselinck, "Inclusion of a direct and inverse energy-consistent hysteresis model in dual magnetostatic finite-element formulations," *IEEE Trans. Magn.*, vol. 52, no. 3, pp. 1–4, 2016.

[47] J. P. A. Bastos, K. Hoffmann, J. V. Leite, and N. Sadowski, "A new and robust hysteresis modeling based on simple equations," *IEEE Trans. Magn.*, vol. 54, no. 3, pp. 1–4, 2018.

[48] C. Geuzaine, F. Henrotte, J.-F. Remacle, and R. V. Sabariego, "ONELAB: Bringing open-source simulation tools to industry design and education," in *Proceedings of the 20th Conference on the Computation of Electromagnetic Fields (COMPUMAG), Montreal, Canada, June 29-July 2, pp. 1–2*, 2015.

[49] C. Geuzaine and J.-F. Remacle, "Gmsh: A 3-D finite element mesh generator with built-in pre- and post-processing facilities," *Int. J. Numer. Methods Eng.*, vol. 79, no. 11, pp. 1309–1331, 2009.

[50] P. Dular and C. Geuzaine, "GetDP reference manual: the documentation for GetDP, a general environment for the treatment of discrete problems," accessed May 2020. [Online]. Available: http://getdp.info

[51] J. Gyselinck and P. Dular, "A time-domain homogenization technique for laminated iron cores in 3D finite element model," *IEEE Trans. Magn.*, vol. 40, no. 3, pp. 1424–1427, 2004.

[52] O. Maloberti, V. Mazauric, G. Meunier, A. Kedous-Lebouc, P. Wendling, and B. Colin, "A magnetic vector potential formulation to deal with dynamic induced losses within 2-D models," *IEEE Trans. Magn.*, vol. 43, no. 4, pp. 1205–1208, 2007.

[53] J. Gyselinck, C. Geuzaine, and R. V. Sabariego, "Considering laminated cores and eddy currents in 2D and 3D finite element simulation of electrical machines," in *Proceedings of the 18th Conference on the Computation of Electromagnetic Fields (COMPUMAG2011)*, Sydney, Australia, July 12–15, 2011.

[54] D. Meeker, "Sliding band motion model for electric machines," accessed May 2020. [Online]. Available: http://www.femm.info/wiki/SlidingBand

[55] B. Scheerlinck, H. De Gersem, and P. Sergeant, "3-D eddy current and fringing-flux distribution in an axial-flux permanent-magnet synchronous machine with stator in laminated iron or smc," *IEEE Trans. Magn.*, vol. 51, no. 11, pp. 1–4, 2015.

[56] P. Handgruber, A. Stermecki, O. Bíró, A. Belahcen, and E. Dlala, "Three-dimensional eddy-current analysis in steel laminations of electrical machines as a contribution for improved iron loss modeling," *IEEE Trans. Ind. Appl.*, vol. 49, no. 5, pp. 2044–2052, 2013.

[57] B. B. Jensen, E. D. Guest, and B. C. Mecrow, "Modeling overlapping laminations in magnetic core materials using 2-D finite-element analysis," *IEEE Trans. Magn.*, vol. 51, no. 6, pp. 1–6, 2015.

Acknowledgement

This work has been partly financed via several projects by the different actors in the Belgian research, namely the Belgian Science Policy, the F.R.S.-FNRS, the FWO, Belgian French and Flemish Communities.

Authors particularly thank Christophe Geuzaine, François Henrotte, Innocent Niyonzima and the late Patrick Dular, former fellow colleagues during their period at the University of Liège, for their valuable contributions to this topic. We would also like to express our high appreciation for the fruitful exchanges with our colleagues Laurent Krähenbühl, Gérard Meunier, Yvonnick Le Menach and Thomas Henneron, that have lead to joint publications on the subject.

Authors name and affiliation

Ruth V. Sabariego, Department of Electrical Engineering, KU Leuven, Campus EnergyVille, 3600 Genk, Belgium.
e-mail: ruth.sabariego@kuleuven.be.

Johan Gyselinck, BEAMS Department, Université Libre de Bruxelles, 1050 Brussels, Belgium.
e-mail: johan.gyselinck@ulb.ac.be.